MMTO Technical Memorandum #03-1

Smithsonian Institution &
The University of Arizona®

Fall 2002 f/9 optical performance of the 6.5m MMT analyzed with the top box Shack-Hartmann wavefront sensor

S. C. West

January 2003

Fall 2002 f/9 optical performance of the 6.5m MMT analyzed with the top box Shack-Hartmann wavefront sensor

MMT Technical Memo #03-1, 17 Jan. 2003

S. C. West
MMTO, Tucson, AZ

Abstract

Some aspects of the f/9 optical performance of the 6.5m MMT as analyzed with the top box Shack-Hartmann wavefront sensor are documented in this memo. The data were collected during Fall 2002. In as few as two "closed-loop" corrections, the diffraction image psf due to the telescope optics is reduced to about 0.1 - 0.2 arcsec. It is shown that the Mirror Lab figure optimization has been successfully correcting about 1.7 microns of primary mirror astigmatism in addition to small amounts of other Zernike mode errors. In additon, we measure about 1.2 microns of trefoil error which repeats well and is removed at the beginning of each night by bending the primary mirror. This error appears to originate with the primary mirror support system. Open-loop corrections for elevation-dependent collimation and focus have been initially characterized. Correcting gravity-induced collimation and focus requires about 70 arcsec of secondary vertex tilt and 300 microns of hexapod focus. "Open-loop" temperature correction (e.g., without the wavefront sensor) remains defiant. This is attributed to relatively poor temperature measuring instrumentation on the OSS, and is in the process of being rectified. At this time, we are still characterizing and correcting the wavefront errors with Zernike polynomials rather than primary mirror bending modes. If a need arises for more efficient bending forces in the future, we may move towards a mirror mode analysis as Magellan has done.

I. Introduction

In 2002, a Shack-Hartmann wavefront analyzer was installed inside the f/9 top box[1]. This location allows the wavefront correction of focus, collimation, and primary mirror figure with any instrument that attaches to the top box. Due to limitations of the old top box and a need to expedite the completion of the unit, it currently analyzes the wavefront only at the telescope optical axis. Therefore, the scientific observations must be interrupted to perform the analysis. This device supplements/replaces a higher resolution stand-alone interferometic wavefront analyzer previously built for the f/9 focus[2,3].

During Fall 2002, about 10 engineering nights were used (in part) to characterize the optical performance of the f/9 telescope. The goals were to determine the repeatable collimation and mirror figure errors so they could be removed in an open-loop fashion (without the wavefront sensor), and to evaluate the closed-loop corrections of the non-repeatable errors.

II. Closed-loop corrections

On 6 nights, shortly after opening the chamber, the wavefront sensor was used to correct both primary mirror figure and collimation errors. The corrections were done in a "closed-loop" fashion where the results of the wavefront analysis were used as a basis for the next correction until the diffraction image was deemed acceptably small. The relationship of primary mirror figure errors to the observed wavefront errors has been previously documented[4,5]. The measured wavefront coma and defocus was related to the hexapod motions empirically (see Appendix A). Figure 1 shows a series of images that illustrate the effectiveness of the top box wavefront corrections on six separate occasions. Each row shows three diffraction images constructed from the observed wavefront errors (with integration times long enough to average atmospheric seeing -- typically 90 sec.). The first column shows the beginning image psf prior to any optical corrections. These wavefront errors are used as the basis of the first correction of primary mirror figure and collimation. The second column shows the psf constructed from the measured wavefront errors after the first corrections. The third column shows that the diffraction images calculated from the wavefront errors measured after the second set of corrections are completely contained within 0.1 - 0.2 arcsec boxes. The conclusion is that as few as two force and collimation iterations significantly improve image quality.

III. Mirror Lab optimization forces

The primary mirror was delivered to the MMTO with a force optimization determined by B. Martin using the Steward Mirror Lab Shack-cube interferometer with the mirror zenith pointing[5]. This force set is shown in Appendix B. We have "blindly" used this optimization each night.

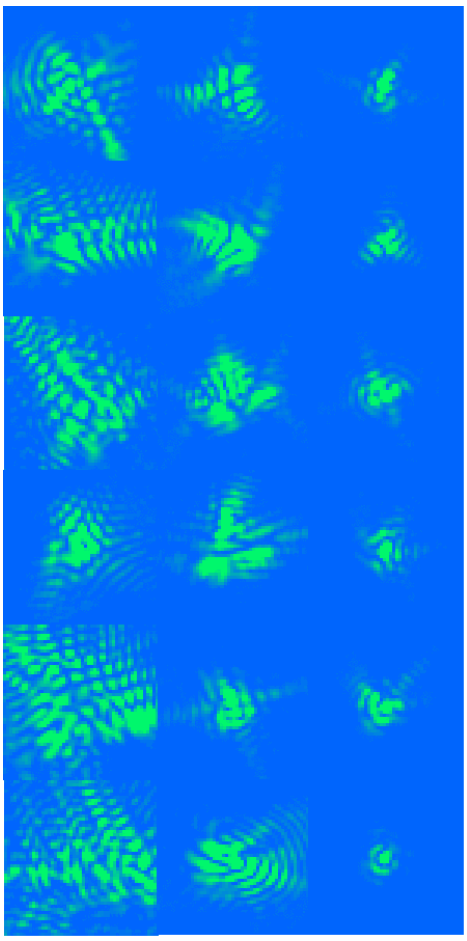

Figure 1: Each row shows two corrections of primary mirror figure and collimation obtained on six nights. The first column shows the starting diffraction image constructed from the initial wavefront errors. The next two columns show the results of each of two corrections of primary mirror figure and secondary collimation. Each psf is shown in a 0.5 x 0.5 arcsec box.

Using the top box wavefront sensor, the wavefront error difference was measured with and without this force set. Table 1

Table 1: Wavefront of Mirror Lab optimization measured with the top box wavefront sensor.

Zernike Mode	Wavefront Amplitude (nm)
astigmatism @ 45-deg	-1000
astigmatism @ 0 deg	+1400
spherical	-43
4-theta_1	+109
4-theta_2	-170
5th order coma X	+70
6th order spherical	+20

shows the results. The corrections do indeed improve each wavefront mode compared to the uncorrected mirror figure. *The mirror lab optimization surface is considered the reference mirror figure* upon which all other wavefront errors are measured.

IV. Repeatable wavefront errors

Since many f/9 instruments do not use the top box, it is advantageous to determine what figure and collimation errors reproduce from night to night. These include primary and secondary mirror errors that are relatively insensitive to thermal state (*e.g.*, support system errors) and collimation errors due to varying gravity on the telescope optical support structure (OSS). Most components of mirror figure error depend greatly upon the thermal state of the borosilicate mirrors, and therefore will always require the wavefront sensor to eliminate.

A. repeatable mirror figure errors

As shown in Figure 2, three mirror figure wavefront errors

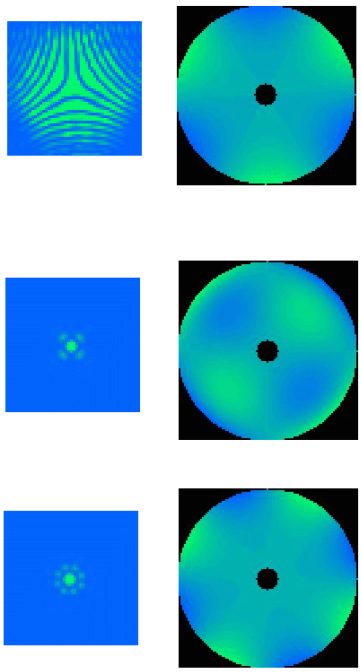

Figure 2: Three f/9 wavefront errors that repeat. The diffraction images corresponding to each mode are shown in 0.5 arcsec boxes (left column), and the corresponding pupil errors are shown at right (north up and east right).

have been determined to repeat to a high degree. The most significant error is $1.2\mu m$ of wavefront trefoil. The pupil map shows that the trefoil is phased onto the primary mirror hardpoint system in the sense that the mirror is “low” directly over the hardpoint pairs. There may be an error in the hardpoint

load cell offsets, but why this was not observed in the mirror lab remains to be explained. The primary mirror as the origin of the trefoil is confirmed since it is observed independent of which secondary mirror is being used (*i.e.*, f/15 or f/9). The other two repeatable components are $290nm$ of 5th-order astigmatism and $250nm$ of 4-theta error.

These three errors are bent into the primary mirror at the beginning of each observing night independent of the availability of the wavefront sensor. Third-order astigmatism is highly variable and can become quite large if the mirror is not in good thermal equilibrium with its environment and spatially isothermal. It and spherical aberration are generally largest at the night's beginning but quickly improve as the thermal management of the mirror improves. Figure 3 shows the diffraction images before and after the application of the open-loop correction forces during the middle of one night. Because the mirror was in good thermal condition, the image was quite good even without any "closed-loop" corrections.

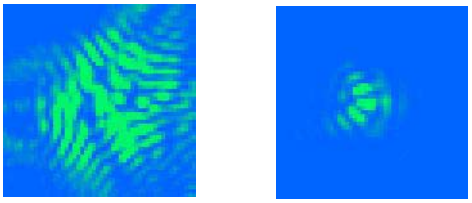

Figure 3: Diffraction images constructed from the measured wavefront errors before (left) and after the removal of the three repeatable figure errors and manual collimation correction. The box size is 0.5 x 0.5 arcsec. The primary mirror was nearly isothermal and at the same temperature as the ambient air.

B. Elevation-dependent collimation and focus

On several nights, the coma and defocus were measured as a function of elevation. The results were averaged and fit to polynomial expressions. The polynomials and residual errors (measured after applying these open-loop corrections) are shown in Figure 4. In order to correct collimation from 30 to 85 degrees elevation, the polynomials apply 75 arcsec of secondary vertex tilt and 300 microns of hexapod focus. Appendix A shows a small amount of coma hysteresis (corresponding to approximately 0.1 arcsec of image diameter) which is currently uncorrected.

As seen in the Figure, the coma correction is very good, but the focus correction requires more work to characterize. A small tool (called elcoll.tcl) was written to apply the polynomial corrections when desired.

C. Correction of focus for temperature changes

Characterizing the elevation-dependent focus is difficult because of changing temperature. As the temperature changes,

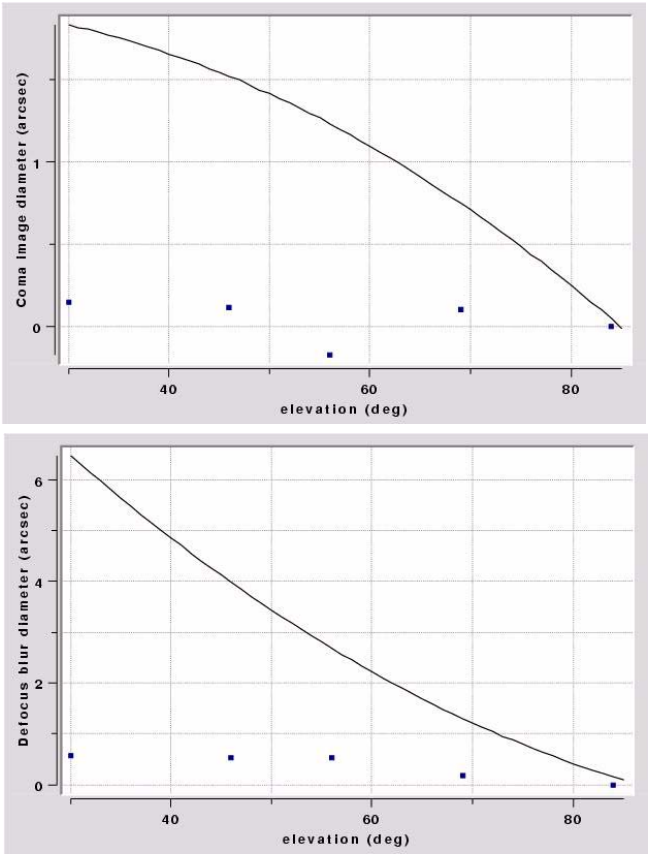

Figure 4: Open-loop polynomial corrections for coma (top) and defocus are shown (solid lines) in terms of angular image diameter. After these corrections are applied to the secondary hexapod, the resulting errors are shown by the small squares (as measured by the wavefront sensor).

the largest contribution to focus error is the length change of the OSS[6]. We have tried unsuccessfully several times to relate focus change to temperature using a single thermocouple mounted within the OSS cavity. We believe that this problem will not be solved until we have more OSS temperature sensors and they are effectively coupled to the steel, insulated from the air, and uncoupled from the sky radiation.

Of course, when the wavefront sensor can be utilized, it corrects for any contribution to focus change. However, since the science observation must be interrupted to measure the wavefront, observing efficiency is maximized if we have excellent open-loop control of focus between these times.

V. Appendix A: Coma and defocus errors

A. Hexapod motion wavefront coefficients

The response of the wavefront to hexapod motions was characterized empirically by moving the hexapod and measuring the wavefront mode amplitudes. Figure 5 shows the wavefront

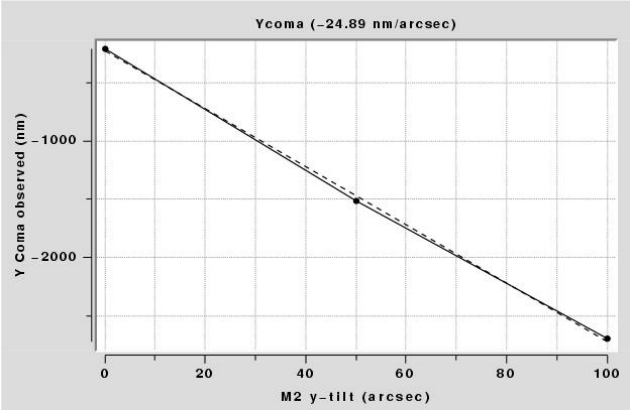

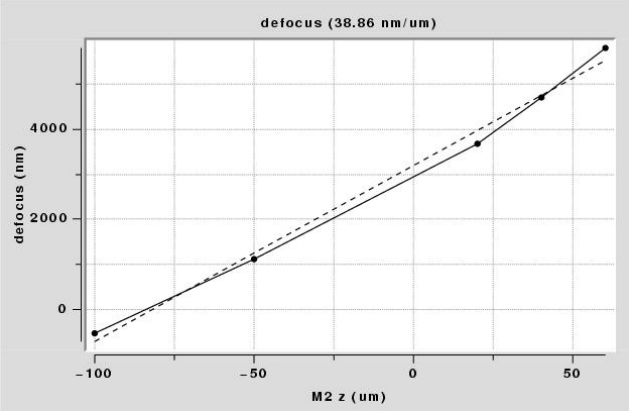

Figure 5: Wavefront amplitude changes vs. hexapod focus and secondary vertex θ_x tilt. Vertex tilt about the y-axis is not shown.

change vs. hexapod focus and secondary mirror vertex tilt changes. Table 2 gives the best-fit line to the response.

Table 2: Emprically determined wavefront amplitude vs. hexapod motion.

Motion	Wavefront ampl/motion
focus	$39nm/\mu m$
vertex rotation about x-axis, Ycoma	$-25nm/''$
vertex rotation about y-axis, Xcoma	$-26nm/''$

B. Elevation coma hysteresis

The elevation-dependent coma along the gravity vector has a small amount of hysteresis which is not included in the open-loop polynomial correction (shown in Figure 6). The Ycoma offset is arbitrary for this graph.

C. Telescope repointing to compensate vertex tilt

When the secondary vertex is tilted to remove on-axis coma, the telescope must be repointed to compensate the wavefront tilt induced. For the f/9 secondary, $\theta_{sky}/\theta_{vertex} = 2/6.69 = 0.3$, where 6.69 is the ratio of the primary to secondary mirror diameters. In practice however, we have found that 0.265 is required for optimum repointing.

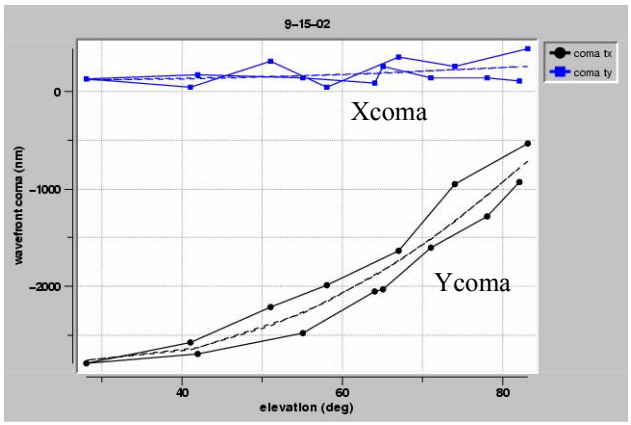

Figure 6: Coma hysteresis vs. elevation corresponding to about 0.1 arcsec image diameter. Polynomial fits shown (dashed).

VI. Appendix B: Mirror Lab force optimization

For inclusiveness, Table 3 lists the Mirror Lab optimization

Table 3: Mirror Lab optimization forces for the primary mirror

Act #	F (N)	Act #	F (N)
1	-22.5	101	-10.8
2	-25.8	102	-14.5
3	-15.3	103	-11.5
4	65.5	104	75.1
5	48.8	105	52.7
6	-33.6	106	-11.9
7	51.4	107	52.4
8	100.7	108	94.2
9	126.6	109	117.4
10	17.4	110	49.8
11	24.5	111	22.7
12	120.2	112	101.8
13	135.7	113	134.3
14	-27.5	114	31.3
15	8.9	115	9.3
16	-13.8	116	-28.5
17	63.4	117	27.1
18	85.9	118	72.7
19	-8.9	119	16.9
20	86.4	120	59.9
21	-35.8	121	-88.8
22	65.8	122	10.3
23	92.9	123	60.3
24	34.0	124	9.3
25	47.8	125	13.9
26	8.6	126	-8.7
27	71.7	127	60.9
28	75.2	128	60.3
29	38.1	129	50.1
30	46.3	130	98.4
31	21.5	131	86.8
32	29.5	132	66.0
33	8.3	133	16.4
34	2.8	134	8.8
35	52.1	135	94.4

Table 3: Mirror Lab optimization forces for the primary mirror

Act #	F (N)	Act #	F (N)
36	24.7	136	93.0
37	-6.0	137	40.1
38	10.4	138	20.4
39	55.3	139	47.7
40	40.9	140	42.1
41	38.0	141	35.9
42	43.8	142	12.3
43	51.4	143	42.7
44	49.5	144	25.4
45	67.1	145	43.6
46	75.6	146	30.5
47	62.9	147	55.8
48	51.2	148	43.5
49	55.5	149	15.0
50	-10.2	150	-11.2
51	13.0	151	13.7
52	32.4	152	23.6

forces, that when added to the baseline BCV forces, define the reference force set for the primary mirror. This optimization is "hardwired" into the VxWorks crate that controls the primary mirror system.

VII. References

[1] S. C. West, S. Callahan, H. Olson, P. Spencer, R. James, R. Ortiz, and T. Pickering, "Design and implementation of a Shack-Hartmann wavefront sensor for the f/9 focus of the 6.5m MMT," *MMT Technical Report* (in progress).

[2] S. C. West, "Interferometric Hartmann wave-front sensing for active optics a the 6.5-m conversion of the Multiple Mirror Telescope", *Applied Optics* **41** #19, 3781-3789 (July 2002).

[3] S. C. West, S. Callahan, and D. Fisher, "An interferometric Hartmann wavefront analyzer for the 6.5m MMT, and the first results for collimation and figure correction," MMT Technical Report #**37**, (11 June 2001).

[4] S. C. West and H. M. Martin, "Correcting 6.5m primary figure errors with the active supports," *MMTO Conversion Technical Memo #**00-2***, (18 Jan. 2000).

[5] H. M. Martin, S. P. Callahan, B. Cuerden, W. B. Davison, S. T. DeRigne, L/ R. Dettmann, G. Parodi, T. J. Trebisky, S. C. West, and J. T. Williams, "Active supports and force optimization for the MMT primary mirror," in *Advanced Technology Optical/IR Telescopes VI*, L. M. Stepp, ed., Proc. SPIE **3352**, 412-423 (1998).

[6] D. Fabricant, B. McLeod, and S. West, "Optical specifications for the MMT conversion," *MMT Technical Report* #**35**, section 8 (21 Dec. 1999).